The Astrophysical Journal, 709:168–178, 2010 January 20 doi:10.1088/0004-637X/709/1/168

HOW ECCENTRIC ORBITAL SOLUTIONS CAN HIDE PLANETARY SYSTEMS IN 2:1 RESONANT ORBITS

Guillem Anglada-Escudé, Mercedes López-Morales[1], and John E. Chambers
Carnegie Institution of Washington, Department of Terrestrial Magnetism, 5241 Broad Branch Rd. NW, Washington, DC 20015, USA;
anglada@dtm.ciw.edu, mercedes@dtm.ciw.edu, chambers@dtm.ciw.edu
Received 2008 September 8; accepted 2009 November 30; published 2009 December 29

ABSTRACT

The Doppler technique measures the reflex radial motion of a star induced by the presence of companions and is the most successful method to detect exoplanets. If several planets are present, their signals will appear combined in the radial motion of the star, leading to potential misinterpretations of the data. Specifically, two planets in 2:1 resonant orbits can mimic the signal of a single planet in an eccentric orbit. We quantify the implications of this statistical degeneracy for a representative sample of the reported single exoplanets with available data sets, finding that (1) around 35% of the published eccentric one-planet solutions are statistically indistinguishable from planetary systems in 2:1 orbital resonance, (2) another 40% cannot be statistically distinguished from a circular orbital solution, and (3) planets with masses comparable to Earth could be hidden in known orbital solutions of eccentric super-Earths and Neptune mass planets.

Key words: celestial mechanics – planetary systems – techniques: radial velocities

Online-only material: color figures, machine-readable table

1. INTRODUCTION

Most of the +300 exoplanets found to date have been discovered using the Doppler technique, which measures the reflex motion of the host star induced by the planets (Mayor & Queloz 1995; Marcy & Butler 1996). The diverse characteristics of these exoplanets are somewhat surprising. Many of them are similar in mass to Jupiter, but orbit much closer to their host stars. This finding has led to extensive work on planet formation and migration theories to explain how those planets got to their present location (e.g., Ward 1997; Ida & Lin 2004). Also, many of the planets seem to move in orbits with eccentricities significantly larger than those observed in the solar system (where $e < 0.1$, except for Mercury which has $e \sim 0.2$). This result poses a problem for the planet formation theories of core accretion (Pollack et al. 1996) and disk instability (Boss 1997), since both predict that planets form in quasi-circular orbits. The current explanation is that large eccentricities are triggered by secular interactions, i.e., the Kozai effect (Soderhjelm 1975), or by rare close-in encounters (Ford et al. 2005). The true distribution of exoplanet eccentricities is therefore key to understand the formation of planetary systems (Thommes et al. 2008).

About 25% of the planets detected to date are in multi-planetary systems. The first multi-planet system was discovered around the solar-type star υ Andromedae (Butler et al. 1997a). Currently, we know of three planets in that system with masses between 0.69 and $3.95 M_J$ and orbital periods between 4.6 and 1275 days. The second multi-planet system discovery was around the M dwarf Gliese 876 (Delfosse et al. 1998). In that case, the first detected planet (Gl 876b, with $M \sin i = 1.935 M_J$ and $P = 60.94$ days) was the one orbiting furthest from the star. A better sampling of the Doppler curve led to the subsequent discovery of the other two planets, Gl 876c, a $0.56 M_J$ planet orbiting with a period of 30.1 days and Gl 876d, a closer-in $0.018 M_J$ planet with a period of only 1.94 days. Gl 876b and c, in particular, are in 2:1 resonance (Laughlin & Chambers 2001).

Interestingly, multi-planet systems are usually first detected as a single planet in a significantly eccentric orbit. Then, every time an additional planet is found, the eccentricities of the already known planets tend to decrease. This is because spurious harmonics due to random noise and uneven sampling are absorbed at half of the period of the detected planet when an eccentric solution is forced (see Lucy 2005 for a more detailed discussion on spurious eccentricities). 55 Cnc (Fischer et al. 2008) and HD 160691(Pepe et al. 2007) are the clearest examples. Both planetary systems started with detections of single massive planets with relatively large eccentricities (i.e., $e > 0.3$). At present, the four planets detected in HD 160691 and the five planets in 55 Cnc have all eccentricities smaller than 0.2. Table 1 illustrates the evolution of the published eccentricities in 55 Cnc as more and more planets were discovered.

In this paper, we explore the case where two-planet systems can be confused with single planets in eccentric orbits. The situation arises when two planets are in a circular 2:1 mean motion resonance being the outer one the most massive ($m_{in}/m_{out} \leqslant 0.5$). Since a full Keplerian solution for a single planet is the natural choice, the statistical degeneracy explained in detail in Section 2 introduces an observational bias toward eccentric solutions. In the forthcoming sections, we show how this bias can have important implications for the known sample of extrasolar planets, that is, a significant fraction of the reported eccentric planets may in fact be multiple systems in nearly circular orbits, and several very low mass planets might have been already detected, but their effect on the star has been misinterpreted as an orbital eccentricity of an outer more massive planet.

2. MATHEMATICAL SOLUTION DEGENERACY

The solution degeneracy between a single-planet eccentric orbit and two planets in circular resonant orbits is a direct consequence of the well-known Fourier expansion of the Kepler equation into powers of the eccentricity (see Moulton 1914, as an example). In Konacki & Maciejewski (1996), the method of frequency analysis was first applied to an extrasolar planetary

[1] Hubble Fellow.

Table 1
Historical Evolution of the Eccentricities in 55 Cnc

Planet	1997[a]	2002[b]	2004[c]	2008[e]
e	...	...	0.174	0.070
b	0.050	0.013	0.019	0.014
c	...	0.080	0.440[c,d]	0.086
f	...	...	...	0.200
d	...	0.146	0.327[c,d]	0.025

Notes.
[a] Butler et al. (1997b). Discovery paper.
[b] Marcy et al. (2002). A second planet is found.
[c] McArthur et al. (2004).
[d] A change of trend is seen here. A different instrument and group were responsible for the discovery of the inner 2.8 day period and the new solution for the outer bodies.
[e] Fischer et al. (2008).

system and Konacki & Maciejewski (1999) adapted it to Doppler measurements. The potential confusion between eccentric orbits and resonant systems has been briefly mentioned in (Marcy et al. 2001) and Ford (2006), but this issue has not been specifically considered until now in a broad statistical sense (Giuppone et al. 2009).

Mathematically, the degeneracy between the resonant and the eccentric solutions comes from the fact that their equations of Keplerian trajectories are identical up to first order in the eccentricity. Detailed analytical expressions in terms of the Bessel functions can be found elsewhere (e.g., Konacki & Maciejewski 1999). The relevant terms up to the 7th power in the eccentricity can be found in Lucy (2005). Here we only discuss the first-order term, which is the one relevant to the degeneracy under discussion

In the case of a single eccentric planet, the reflex radial velocity motion of the star is

$$v_r^e = v_{r0} + K\cos\left[W\left(t-\tau_0\right)\right] + Ke\cos\left[2W\left(t-\tau_0\right)-\omega\right] + O(Ke^2)\,, \quad (1)$$

where v_{r0} is the linear radial velocity of the barycenter of the system, K is the semi-amplitude of the radial velocity variations induced by the planet on the star, ω is the argument of the periastron (angle between the periastron of the orbit and the ascending node), τ_0 is the time of crossing of the ascending node, and $W = 2\pi/P$ is the orbital frequency, where P is the orbital period (see Figure 1(a)). The term proportional to Ke is called the first eccentric harmonic, while the term $O(Ke^2)$ contains all the higher order contributions.

If instead we have a two-planet system, both in circular orbits and the inner planet having an orbital period half of the outer one, i.e., $W_2 = 2W$ (see Figure 1(b)), the expression for the radial velocity of the star is

$$v_r^R = v_{r0} + k_1\cos\left[W\left(t-\tau_0\right)\right] + k_2\cos\left[2W\left(t-\tau_0\right)+\phi_0\right] + O(k_1e_1, k_2e_2, Ke^2), \quad (2)$$

where k_1 and k_2 are the radial velocity semi-amplitudes of the outer and the inner planets. W and τ_0 are the orbital frequency and the time of crossing of the ascending node of the outer planet, and the angle ϕ_0 is the relative phase between the two planets at τ_0. Higher order terms, summarized here as

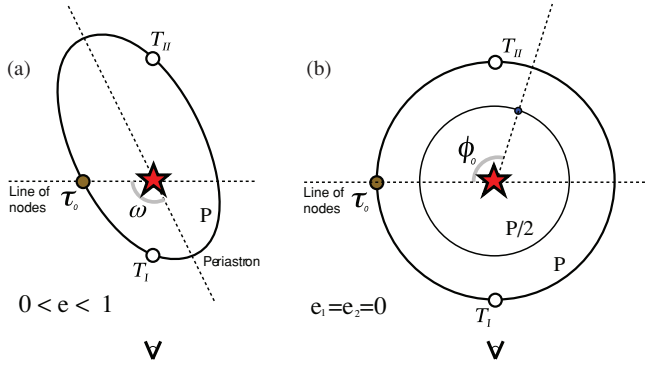

Figure 1. Seen from *above*, diagrams of the relevant orbital parameters of one planet in an eccentric orbit (left), and two planets in a 2:1 resonant circular orbit (right). τ_0 is the instant of crossing of the line of nodes. The instants of transit and occultation are marked as $T_{\rm I}$ and $T_{\rm II}$.
(A color version of this figure is available in the online journal.)

$O(k_1e_1, k_2e_2, Ke^2)$, become significant if the orbits are allowed to be eccentric.

To a first-order approximation, v_r^e and v_r^R are formally identical if $k_1 = K$, $k_2 = Ke$, and $\phi_0 = -\omega$. This implies that the signal k_2 of an inner lower mass planet will be indistinguishable from the first eccentric harmonic Ke unless the observations are precise enough to resolve the second-order term in the harmonic expansion. The amplitude of that second-order term is $9/8\,Ke^2 \sim Ke^2$. (see Appendix A in Lucy 2005).

The similarity of both solutions is illustrated in Figure 2, which shows how the Doppler radial velocity curves would look like in each case (one-planet in an eccentric orbit versus two resonant planets in circular orbits), for different values of ω and e. The two configurations can be easily confused, especially when $e < 0.3$ in the single-planet case (or equivalently, when the inner planet is significantly less massive than the outer planet, i.e., $k_2 \ll k_1$). Confusion is also possible for larger values of e if the uncertainties are large and the radial velocity curves are sparsely sampled, which is the case for several published Doppler velocity curves. As an example estimate, if the detected semi-amplitude and eccentricity are $K \sim 100\,{\rm m\,s^{-1}}$ and $e \sim 0.1$, the amplitude of the second harmonic will be $Ke^2 \sim 1\,{\rm m\,s^{-1}}$ and both orbital solutions are indistinguishable at the 3σ level unless the precision of the data is better than 0.3 m s^{-1}. This is a problem, since only recently have planet hunting groups started to achieve that level of precision (Mayor et al. 2009a; Fischer et al. 2008). All these statements will be made more precise in Section 3.1. There is also the accuracy limitation imposed by the stellar jitter,[2] which has typical amplitudes of 3–5 m s^{-1} (Cumming et al. 2008). The optimal strategies and the limitations of the Doppler technique to disentangle this degeneracy are discussed in Section 5.

3. IMPACT ON KNOWN PLANETARY SYSTEMS

Since at least 200 of the 350 known exoplanets have reported eccentricities between 0.03 and 0.5, the mathematical degeneracy described in the previous section may be affecting a large fraction of known reported planets in eccentric orbits. Of course, this does not imply that all the reported eccentric solutions must be resonant pairs instead, but a significant fraction of them may be, and this can have a strong impact on our understanding of formation of planetary systems.

[2] Intrinsic noise associated to the stellar activity.

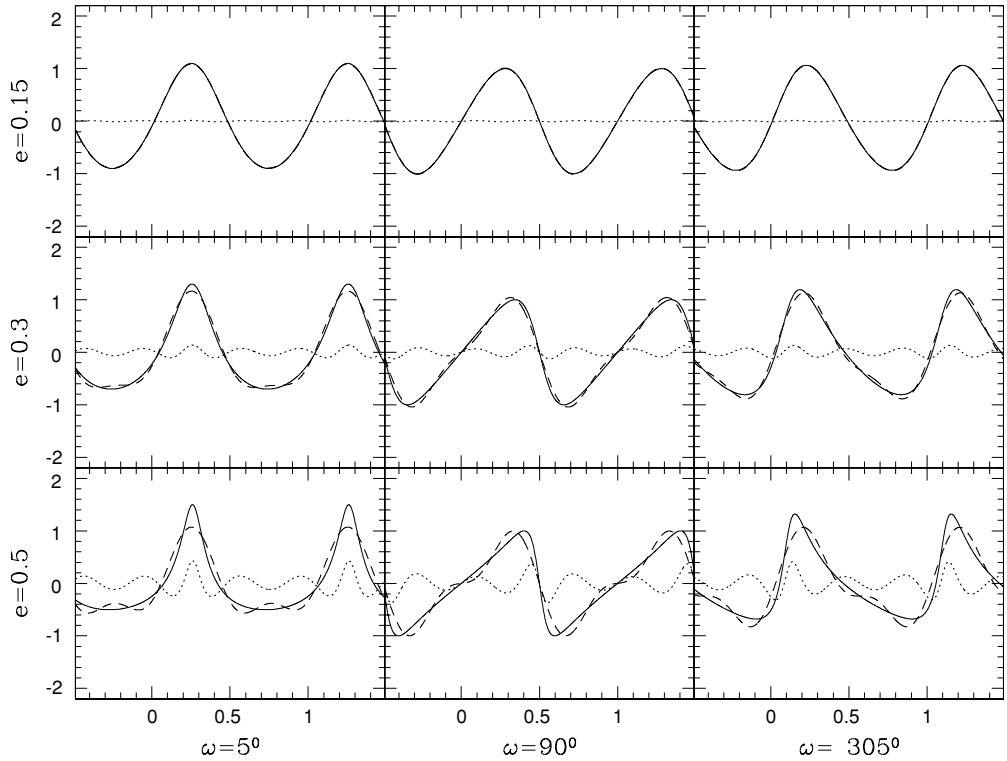

Figure 2. Radial velocity signals normalized to $K = 1$. The eccentric solution is the black solid line (Equation (1)). The dashed line corresponds to the resonant case (Equation (2)). The difference is clearly shown by the dotted line. In cases where $e < 0.3$, both cases are hardly distinguishable (top panels).

Table 2
List of Planets with Reported Eccentricities

Planet	$m \sin i$ ($m_\oplus$)	P (days)	e	K (m s^{-1})	Ke (m s^{-1})	Ke^2 (m s^{-1})	$m_h \sin i$ ($m_\oplus$)
GJ 581 c	5.06	12.93	0.17	3.38	0.58	0.10	0.68
GJ 581 d	6.69	66.80	0.38	2.76	1.05	0.40	2.02
HD 181433 b	7.14	9.37	0.40	3.08	1.22	0.48	2.24
HD 7924 b	8.70	5.40	0.17	4.03	0.69	0.12	1.17
HD 69830 b	9.90	8.67	0.10	3.80	0.38	0.04	0.79
HD 160691 c	9.96	9.64	0.17	3.20	0.55	0.09	1.36
55 Cnc e	10.20	2.82	0.07	5.03	0.35	0.02	0.57
GJ 674 b	11.10	4.69	0.20	9.65	1.93	0.39	1.76
HD 69830 c	11.40	31.56	0.13	2.85	0.37	0.05	1.18
HD 190360 c	17.10	17.10	0.01	4.58	0.05	0.00	0.14
...	...	...	...	...	...	...	...

Notes. Data extracted from the Extrasolar Planet Encyclopedia (http://exoplanet.eu, maintained by J. Schneider).

(This table is available in its entirety in a machine-readable form in the online journal. A portion is shown here for guidance regarding its form and content.)

Assuming circular orbits, the mass of the inner companion candidate m_h can be estimated from the Keplerian solution as

$$m_h \sin i = \frac{e}{2^{1/3}} m_1 \sin i, \tag{3}$$

where m_1 is the mass of the outer planet and e is its eccentricity, both parameters derived from the one-planet fit. The $\sin i$ factor reflects the fact that the inclination i (and the true mass) is unknown when only Doppler information is available. When a resonant two-planet system is confused with a single eccentric planet, we refer to this situation as an eccentricity imposter. The term Ke^2 in Table 2 gives the amplitude of the signal that needs to be resolved in all radial velocity candidates to distinguish between solutions.

3.1. Statistical Analysis

In order to quantify the extent of this degeneracy in the currently known planet sample, we performed actual fits to most of the known candidates with available data up to the date (2009 March, see the Exoplanet Encyclopedia[2]). The data have been collected from two sources, the systemic project web page *Systemic*[3] (Meschiari et al. 2009), and the NStED database.[4] Still, there is a significant number of published detections with no publicly available data sets. The transiting exoplanets have been excluded from the list because many of them have poorly sampled radial velocity curves, and their true eccentricity can be determined by other means such as the photometric methods as described in Section 5.2. Known multi-planetary systems have been excluded from the list as well. These systems require a more complex analysis which adds unnecessary complications at this point. A number of highly eccentric planets have not been added in the main sample because there is no reasonable doubt about their eccentric nature. Their eccentricities, their corresponding Ke^2, and the signal-to-noise ratio (S/N) of the second eccentric harmonic are given in Table 4, and they are included in the statistical discussion at the end of this section. The sample processed by our orbital fitting approach contains 163 data sets listed in Table 3.

Our method is based on a sequential fit of three different models: circular, resonant, and finally Keplerian. This approach takes maximum advantage of the epicyclic decomposition of the radial velocity signal as given in Equation (1). For practical purposes, Equation (1) can be written as

$$\begin{aligned} v_r^e = \gamma &+ A \sin(Wt) + B \cos(Wt) \\ &+ C \sin(2Wt) + D \cos(2Wt) \\ &+ \beta t, \end{aligned} \tag{4}$$

[3] http://oklo.org, maintained by G. Laughlin.
[4] http://nsted.ipac.caltech.edu/

Table 3
Statistical Comparison of Circular, Resonant, and Eccentric Orbital Solutions

Planet	$\sqrt{\chi_c^2}$	$\sqrt{\chi_r^2}$	$\sqrt{\chi_e^2}$	NC c.l.	$N_{\rm obs}/N_{\rm req}$	Preferred	FAP (%)	Quality
6 Lyncis	1.67	1.64	1.64	76.88	30	Circular	...	
14 And	3.37	3.49	3.49	0.02	34	Circular	...	
14 Her	3.43	1.86	1.60	99.99	119/30	Eccentric	10.00	U
16 CygB	3.14	2.58	1.22	99.99	95/1	Eccentric	0.20	**
18 Del	2.27	2.22	2.23	85.85	51	Circular	...	
42 Dra	8.57	7.29	7.02	99.98	45/763	Eccentric	∼50.0	U
51 peg	1.02	1.02	1.02	49.51	256	Circular	...	
70 vir	14.94	6.93	1.33	99.99	74/1	Eccentric	0.00	***
81 Ceti	2.10	1.76	1.69	99.89	33/361	Eccentric	∼50.0	U
β Gem	2.21	2.19	2.18	86.34	80	Circular	...	
BD-10 3166	1.55	1.58	1.58	39.39	31	Circular	...	
ChaHa8	0.92	0.89	0.88	76.72	15	Circular	...	
ϵ Eri	2.29	2.29	2.25	96.03	120/150[a]	Eccentric	0.10	***
GJ 176	3.58	3.56	3.48	90.57	57	Circular	...	
GJ 3021	5.66	3.49	1.86	99.99	61/21	Eccentric	0.00	***
GJ 849	1.62	1.62	1.62	64.53	29	Circular	...	
HD 142	1.11	0.81	0.79	99.97	27/47	Eccentric	50.00	U
HD 2638	2.23	2.30	2.30	27.13	28	Circular	...	
HD 3651	2.54	2.12	2.04	99.99	121/10	Eccentric	4.00	*
HD 4203	4.77	2.39	1.29	99.99	23/1	Eccentric	0.00	***
HD 4208	1.17	1.17	1.18	69.01	41	Circular	...	
HD 4308	1.36	1.34	1.35	78.26	41	Circular	...	
HD 5319	3.36	3.33	3.35	70.49	30	Circular	...	
HD 6434	1.52	1.40	1.41	99.99	130/+1000	Resonant	6.50	U
HD 7924	3.81	3.77	3.78	83.83	93	Circular	...	
HD 8574	1.69	1.32	1.13	99.99	41/148	Eccentric	∼50.00	U
HD 10647	1.56	1.53	1.56	87.85	70	Circular	...	
HD 10697	3.99	2.39	2.48	99.99	59/415	Resonant	∼50.00	U
HD 11977	1.43	1.15	1.15	99.99	42/+1000	Resonant	34.0	U
HD 12661	2.91	2.02	2.13	99.99	51/+1000	Resonant	15.00	U
HD 13189	12.01	9.79	10.23	99.99	91/+1000	Resonant	3.30	*
HD 13445	3.56	2.67	2.68	99.99	42/+1000	Resonant	∼50.00	U
HD 14810	45.96	24.65	22.13	99.99	30/+1000	Eccentric	∼50.00	U
HD 16141	1.64	1.49	1.47	99.96	71/+1000	Eccentric	∼50.00	U
HD 16417	3.73	3.50	3.53	99.77	88	Resonant	∼50.00	U
HD 19994	1.88	1.56	1.56	99.98	48/458	Eccentric	19.00	U
HD 20367	1.29	1.19	1.24	93.49	27	Circular	...	
HD 17092	3.11	2.95	2.95	97.58	59/+1000	Eccentric	∼50.00	U
HD 23079	1.05	0.82	0.90	98.31	19/813	Resonant	∼50.00	U
HD 23127	3.54	3.14	2.85	99.91	34/152	Eccentric	29.00	U
HD 24040	3.64	3.56	3.55	77.40	26	Circular	...	
HD 27442	4.22	3.97	3.96	98.39	55/+1000	Eccentric	∼50.00	U
HD 27894	2.57	2.49	2.47	78.78	20	Circular	...	
HD 28185	1.67	1.60	1.59	92.89	40	Circular	...	
HD 28185	1.44	1.51	1.51	42.72	15	Circular	...	
HD 28305	2.71	2.26	2.17	98.40	20/800	Eccentric	∼50.00	U
HD 30177	1.31	1.16	1.15	88.35	15	Circular	...	
HD 33283	1.44	0.82	0.76	99.99	25/39	Eccentric	40.00	U
HD 33636[c]	8.84	2.46	1.41	99.99	21/1	Eccentric	0.00	***
HD 39091	19.40	10.88	1.29	99.99	42/1	Eccentric	0.00	***
HD 81688	4.00	3.98	3.75	93.74	34	Circular	...	
HD 88133	1.57	1.43	1.51	86.87	17	Circular	...	
HD 40979	2.69	2.04	1.96	99.99	39/+1000	Eccentric	∼50.00	U
HD 41004B	1.12	1.01	0.99	99.99	149/+1000	Eccentric	∼50.00	U
HD 43691	1.28	1.26	1.27	70.36	22	Circular	...	
HD 43848	7.68	0.57	1.57	99.99	10/1[b]	Resonant	0.00	***
HD 46375	1.77	1.72	1.72	88.86	50	Circular	...	
HD 48265	1.53	1.47	1.49	74.82	17	Circular	...	
HD 49674	1.56	1.60	1.60	26.89	39	Circular	...	
HD 50499d	1.03	1.06	1.06	31.51	28	Circular	...	
HD 50554	3.75	2.42	1.31	99.99	40/20	Eccentric	3.90	*
HD 52265	1.47	1.15	1.14	99.99	91/117	Eccentric	26.00	U
HD 63454	2.85	2.62	2.59	94.72	26	Circular	...	
HD 64468	266.72	30.94	4.28	99.99	13/1	Eccentric	0.00	***
HD 65216	1.63	1.27	1.22	99.99	70/40	Eccentric	15.00	U
HD 66428	4.30	2.08	1.10	99.99	29/1	Eccentric	4.80	*

Table 3
(Continued)

Planet	$\sqrt{\chi_c^2}$	$\sqrt{\chi_r^2}$	$\sqrt{\chi_e^2}$	NC c.l.	$N_{\rm obs}/N_{\rm req}$	Preferred	FAP (%)	Quality
HD 68988	7.00	4.54	4.48	99.99	28/+1000	Eccentric	∼50.00	U
HD 70573	2.02	2.06	2.03	54.80	34	Circular	...	
HD 70642	1.30	1.31	1.31	59.61	28	Circular	...	
HD 72659	1.87	1.85	0.00	59.61	28	Circular	...	
HD 73108	12.46	6.46	5.46	99.99	59/104	Eccentric	7.50	U
HD 73267	5.25	1.40	1.15	99.99	39/1	Eccentric	0.01	***
HD 75289	0.86	0.86	0.86	52.20	88	Circular	...	
HD 76700	1.33	1.28	1.28	85.94	35	Circular	...	
HD 81040	2.70	2.53	2.00	99.91	26/115	Eccentric	∼50.00	U
HD 83443	1.64	1.64	1.64	31.80	257	Circular	...	
HD 86081	1.14	1.03	1.03	95.11	26/+1000	Resonant	∼50.00	U
HD 88133	1.98	1.89	1.96	81.68	21	Circular	...	
HD 89307	0.62	0.52	0.55	86.41	12	Circular	...	
HD 89744	8.57	6.57	1.44	99.99	85/3	Eccentric	0.00	***
HD 92788	3.47	2.27	1.63	99.99	55/25	Eccentric	3.60	*
HD 93083	2.15	1.76	1.75	95.28	16/47	Eccentric	∼50.00	U
HD 99109	1.62	1.66	1.66	17.54	41	Circular	...	
HD 99492	1.43	1.32	1.34	98.69	51/122	Resonant	∼50.00	U
HD 100777	4.06	1.71	1.22	99.99	29/5	Eccentric	10.00	U
HD 101930	2.09	2.17	2.20	45.74	16	Circular	...	
HD 102117	1.05	1.05	1.05	55.34	44	Circular	...	
HD 102195	1.18	1.18	1.34	65.49	21	Circular	...	
HD 104985	4.32	4.15	4.12	95.85	52/+1000	Eccentric	∼50.00	U
HD 106252	4.41	1.98	1.11	99.99	40/9	Eccentric	0.00	***
HD 107148	1.47	1.51	1.52	20.65	35	Circular	...	
HD 108147	2.07	1.60	1.33	99.99	118/80	Eccentric	0.00	***
HD 109749	1.08	1.04	1.04	78.12	21	Circular	...	
HD 114386	1.74	1.50	1.59	99.99	58/+1000	Resonant	40.00	U
HD 114729	1.63	1.58	1.53	96.33	42/82	Eccentric	42.00	U
HD 114762	6.90	2.88	1.08	99.99	45/23	Eccentric	0.00	***
HD 114783	1.82	1.77	1.77	89.45	54	Circular	...	
HD 117207	1.38	1.23	1.25	99.35	43/739	Resonant	27.00	U
HD 117618	1.43	1.41	1.35	97.93	57/73	Eccentric	30.00	U
HD 118203	3.60	1.90	1.50	99.99	43/147	Eccentric	17.00	U
HD 121504	1.92	1.93	1.93	52.03	100	Circular	...	
HD 125612	13.77	2.16	4.82	99.99	19/21	Resonant	0.03	***
HD 130322	1.33	1.29	1.29	98.85	118/+1000	Eccentric	30.00	U
HD 134987	3.60	1.83	1.68	99.99	56/30	Eccentric	15.00	U
HD 136118	2.96	1.48	1.25	99.99	37/101	Eccentric	3.40	*
HD 139357	1.91	1.75	1.75	99.20	49/+1000	Resonant	45.00	U
HD 141937	4.06	2.29	1.58	99.99	81/2	Eccentric	0.10	***
HD 142022A	2.40	1.57	1.37	99.99	49/13	Eccentric	0.80	**
HD 142091	2.24	2.28	2.26	53.81	46	Circular	...	
HD 143361	1.95	0.85	1.24	97.54	12/13	Resonant	8.00	U
HD 145377	26.00	10.87	9.02	99.99	64/50	Eccentric	40.00	U
HD 147513	1.88	1.63	1.59	99.35	30/349	Eccentric	33.00	U
HD 149026	3.11	3.18	3.17	40.26	30	Circular	...	
HD 149143	1.16	1.15	1.15	67.07	17	Circular	...	
HD 150706	0.98	0.82	0.76	98.47	19/183	Eccentric	∼50.00	U
HD 153950	6.67	3.03	2.42	99.99	49/20	Eccentric	40.00	U
HD 154345	2.77	2.70	2.65	95.43	55/194	Eccentric	∼50.00	U
HD 154672	8.68	5.06	1.80	99.99	16/1	Eccentric	0.01	***
HD 154857	11.39	8.19	8.54	99.97	28/726	Resonant	∼50.00	U
HD 160691	5.78	4.45	4.25	99.99	108/46	Eccentric	1.10	*
HD 162020	32.32	7.82	1.61	99.99	46/2	Eccentric	0.00	***
HD 164922	1.57	1.59	1.59	22.99	64	Circular	...	
HD 167042	1.51	1.57	1.57	1.76	31	Circular	...	
HD 167042	1.28	1.33	1.33	14.13	29	Circular	...	
HD 168746	1.50	1.50	1.50	79.29	154	Circular	...	
HD 169822	20.44	5.64	1.67	99.99	21/1	Eccentric	0.00	***
HD 170469	2.38	2.44	2.43	28.36	35	Circular	...	
HD 173416	1.71	1.50	1.50	99.90	52/+1000	Resonant	∼50.00	U
HD 175541	2.80	2.66	2.57	94.80	29	Circular	...	
HD 177830	3.21	3.14	3.14	87.75	54	Circular	...	
HD 178911B	2.76	1.13	1.06	99.99	44/187	Eccentric	∼50.00	U
HD 179949	2.16	2.15	2.15	72.02	65	Circular	...	

Table 3
(Continued)

Planet	$\sqrt{\chi_c^2}$	$\sqrt{\chi_r^2}$	$\sqrt{\chi_e^2}$	NC c.l.	N_{obs}/N_{req}	Preferred	FAP (%)	Quality
HD 185269	3.08	2.07	1.74	99.99	30/68	Eccentric	∼50.00	U
HD 188015	1.80	1.44	1.44	99.99	44/248	Eccentric	∼50.00	U
HD 189733	7.33	6.15	6.12	93.88	16	Circular	...	
HD 190228	2.84	1.36	0.98	99.99	51/4	Eccentric	0.10	***
HD 190647	2.41	1.00	1.24	99.99	21/9	Resonant	10.00	U
HD 192263	1.64	1.65	1.65	43.98	181	Circular	...	
HD 192699	1.97	1.90	1.89	89.53	34	Circular	...	
HD 195019	1.66	1.67	1.67	42.31	117	Circular	...	
HD 196050	2.62	1.79	1.65	99.99	44/103	Eccentric	29.00	U
HD 205739	2.99	2.51	2.83	98.45	24/348	Resonant	∼50.00	U
HD 208487	1.63	1.49	1.47	98.08	35/356	Eccentric	∼50.00	U
HD 209458	1.60	1.61	1.61	6.39	141	Circular	...	
HD 210277	5.03	3.07	1.61	99.99	69/1	Eccentric	0.00	***
HD 210702	1.64	1.61	1.59	80.38	29	Circular	...	
HD 212301	2.39	2.14	2.11	95.41	23/+1000	Eccentric	∼50.00	U
HD 213240	3.10	1.78	1.84	99.99	72/30	Resonant	2.80	*
HD 216435	1.71	1.74	1.74	14.41	58	Circular	...	
HD 216437	3.23	1.61	1.60	99.99	39/25	Eccentric	39.00	U
HD 216770	1.32	1.23	1.11	93.40	16	Circular	...	
HD 224693	1.27	1.31	1.30	47.66	24	Circular	...	
HD 231701	1.84	1.87	1.84	63.22	17	Circular	...	
HD 330075	1.43	1.52	1.52	7.73	21	Circular	...	
HIP 75458	27.84	21.44	3.15	99.99	119/1	Eccentric	0.00	***
HR 810	1.68	1.56	1.54	99.99	95/+1000	Eccentric	40.00	U
ksi Aquila	3.85	3.71	3.58	91.42	26	Circular	...	
NGC 2423 3	2.76	2.48	2.41	98.00	28/+1000	Eccentric	∼50.00	U
NGC 4349 127	6.75	6.45	6.23	88.14	20	Circular	...	
ρ CrB	1.11	1.08	1.07	97.24	79/+1000	Eccentric	27.00	U
τ Boo	1.92	1.91	1.91	65.51	98	Circular	...	

Notes. The quality column highlights the significance of the solution : "***" is a secure solution, U indicates undecided. The estimated number of required observations to detect the second harmonic N_{req} is only given if the orbital solution is significantly non-circular.

[a] Other data sets and astrometry seem to confirm the eccentricity. Very noisy star.

[b] The obtained solution differs from the published one significantly.

[c] According to (Bean et al. 2007), astrometric observations indicate that the candidate is a star indeed with an orbital inclination close to 0.

which shows that the only severe nonlinearity on the expression for the Doppler Keplerian signal is in the period. All the other orbital parameters can be obtained as combinations of the coefficients using basic trigonometric identities. The parameter β takes into account the signal of very long-period objects which appear as a linear trend. It is usually fitted to the published solution, and we will keep it as a free parameter in all that follows.

Step 1 consists of doing a linear least-squares (LS) fitting of γ, A, B, and β for many test periods. The best period is the one which gives the minimum χ^2. This is equivalent to the classic Lomb–Scargle periodogram, but has the advantage that the peaks (LS minima in this case) and the coefficients from the fit have a direct physical interpretation (see Cumming 2004, for a review on the topic).

In the second step, the data are fitted against the more complete model containing γ, A, B, C, D, and β using many test periods around the best circular solution found in step 1. Let us remark again that the only strong nonlinearity lies on the period, so the fitting of the linear parameters can be done very efficiently and without danger of ending in a local minimum, a problem which plagues more direct attack methods. The solution of this step gives the best resonant orbital solution.

Finally, the exact Keplerian expression for the radial velocity (see Lucy & Sweeney 1971) is fitted to the data using a nonlinear LS approach. The seed values of the parameters for the Keplerian solution are obtained from the resonant solution using the map defined by Equations (1) and (2). The optimal Keplerian fit is done using a straightforward nonlinear LS minimization scheme using the analytic partial derivatives of the Doppler signal with respect to the orbital parameters (Press et al. 1992). The final Keplerian fits we obtain are in good agreement with those found in the literature. Therefore, as a by-product of this study, we also proof a powerful method to attack the Kepler problem taking advantage of the Linearized form of the Keplerian motion. The $\sqrt{\chi^2}$ of each solution (circular, resonant, and eccentric) is shown in Columns 2–4 of Table 3.

The next step is to decide which of the orbital solutions is the best (resonant or Keplerian) and whether it is significantly better than the circular one. To do this, we apply the confidence level test given by Lucy & Sweeney (1971) and Lucy (2005). We only accept one of the non-circular solutions if the c.l. is better than 95%.

In order to decide if the best non-circular solution (e.g., resonant) is statistically better than the other one (e.g., Keplerian), we compute the false alarm probability (FAP) of the favored solution as follows. Let us assume that the resonant solution is preferred, i.e., $\sqrt{\chi^2_{res}} < \sqrt{\chi^2_{ecc}}$. Then we generate a synthetic data set using the best Keplerian solution. We add Gaussian noise with a standard deviation equal to the RMS of

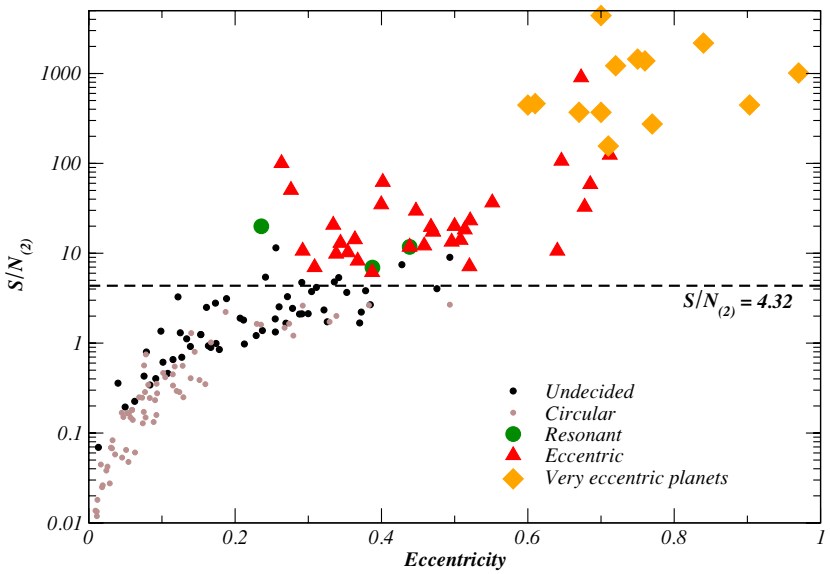

Figure 3. Orbital eccentricity vs. the signal-to-noise ratio of the Ke^2 harmonic. Only systems above the 4.32 dashed line can be statistically distinguished. The black dots are solutions where the eccentric/resonant fit is significantly better than the circular one but cannot be decided which solution is favored.
(A color version of this figure is available in the online journal.)

the Keplerian fit, and then obtain the best-fit resonant configuration. This process is repeated a large number of times. The number of times when we get a $\sqrt{\chi^2}$ smaller than the real resonant solution illustrates how an (un)fortunate combination of random errors may be confusing a truly eccentric orbit with a resonant one. In contrast, if the eccentric solution is preferred, we generate synthetic resonant data and fit for the Keplerian solution. Since this is a computationally expensive process, the FAP is initially computed based on 1000 synthetic realizations of the data. If the FAP is found to be smaller than 10%, the FAP is recomputed using 10^5 data sets. The result of this process is illustrated in the last three columns of Table 3, which contains the preferred model, its FAP, and a quality indicator: "*" indicates a FAP <5%, "**" corresponds to FAP <1%, and "***" is FAP <0.1%. If the solutions are not significantly different (FAP >5%) they are flagged as U (*undecided*).

The results of this procedure are also illustrated in Figure 3. The quantity on the *y*-axis is defined as the S/N of the second harmonic and is computed from the best Keplerian fit as

$$\mathrm{S/N}_{(2)} = \frac{K e^2}{\mathrm{RMS}} \sqrt{N_{\mathrm{obs}}}, \qquad (5)$$

where RMS is the root mean square of the residuals, and N_{obs} is the number of observations. The horizontal line at $\mathrm{S/N}_{(2)} = 4.32$ is the minimal theoretical threshold to detect the second Keplerian harmonic, assuming that the required level of significance p is 95% as given in Lucy (2005, Equation (18)). The black points are the undecided ones, that is, where the first eccentric harmonic is clearly significant (circular solution discarded), but the statistics are insufficient to decide which solution is significantly better (eccentric versus resonant).

A word of caution has to be made here. The $\sqrt{\chi^2}$ are obtained using the nominal uncertainties published with the Doppler data. It is well established that most of the stars introduce additional noise of the astrophysical origin, that is usually called stellar jitter. The jitter makes it more difficult to disentangle the degeneracy under discussion, meaning that more accurate measurements with better spectrographs may not help. In the randomly generated data sets, not considering the noise due to the stellar jitter tends to give overoptimistic FAP. This is the reason why we use the RMS of the solution rather than the published uncertainties to generate synthetic data.

In many cases, the current radial velocity data sets are sparsely sampled, and more intensive monitoring at the most sensitive phases is required (see Section 5.1), especially for those systems above the 4.32 line of Figure 3 and marked in Table 3 as undecided. We also show how the number Ke^2 is a powerful discriminator to a priori evaluate if a data set is sensitive to the second eccentric harmonic, or equivalently, if a data set is able to disentangle the degeneracy under discussion by just computing $\mathrm{S/N}_{(2)}$ using the Keplerian parameters. In all the cases where an eccentric/resonant solution is preferred against a circular one, we have added to Column 6 in Table 3 the number of required observations N_{req} to reach the $\mathrm{S/N}_{(2)}$ of 4.32 according to the eccentricity and RMS of the best Keplerian solution using Equation (5). A circular orbit means that the first eccentric harmonic proportional to Ke is already too small to be detected, so N_{req} is not given. In many cases, the number of required observations is extremely large. These cases are indicated with a +1000. Even if the minimum number of observations is reached, it is not always possible to distinguish between solutions depending on the sampled phase. In such cases, a few more points in the right phases should be enough to confirm a resonant candidate or a given eccentricity. It is also important to note that extending the time baseline can help disentangle resonant systems if the periods are not exactly 2:1 or if the system is in a strong interacting regime. This point is discussed again in Section 4.

Our results considering the sample of 163 planets plus the 13 very eccentric ones in Table 4 are shown in Table 5. When the solution is clearly non-circular, our data processing approach is unable to determine which solution is favored in 63% of the cases, which clearly proves the extent of the degeneracy. The statistical behavior of the sample is in good agreement with the predicted degeneracy threshold at $\mathrm{S/N}_{(2)} = 4.32$. This gives us confidence in our data analysis scheme and the method we

Table 4
Already Known Eccentric Planets Not Included in Table 3

Planet	e	Ke^2	$S/N_{(2)}$
HD 4113	0.903	335	446
HD 156846	0.84	2100	2181
HD 20782	0.97	438	1012
HD 222782	0.76	924	1380
HD 20868	0.75	355	1446
HD 75458	0.72	1496	1218
HD 96167	0.71	115	156
HD 159868	0.7	279	369
HD 2039	0.67	785	370
HD 37605	0.77	370	274
HD 131664	0.7	2757	4413
HD 171028	0.61	618	462
HD 16175	0.6	618	445

propose to evaluate the statistical significance of each solution using Monte Carlo generated FAP. A few systems with already known resonant configurations that have gone to the process—detect one eccentric planet and later discovery of a second planet in a 2:1 configuration—are not considered in these counting (e.g., GJ 876 with three known planets, HD 128311 with two planets, HD 160691 with four planets). With this, we want to remark that highly eccentric candidates with unexplained large RMS (with large χ^2 in Table 3) seem to be good targets to follow up and uncover multi-planetary systems with very low mass companions.

3.2. HD 125612b/c?

A detailed analysis of our best resonant candidate system HD 125612 is discussed here to illustrate the procedure of evaluating the FAP in more detail. HD 125612b is a gas giant planet detected around a nearby G3V star as reported by Fischer et al. (2007, from now on F07). A common proper motion M4V companion has been recently associated with the system (Mugrauer & Neuhäuser 2009). The M4V is at a minimum distance of ∼4750 AU from HD 125612A and has negligible effects on the Doppler data during the time span of the observations. The star is relatively quiet, so the expected jitter is of the order of 2.0 m s^{-1}. F07 already pointed out an unexpectedly large RMS and $\sqrt{\bar{\chi}^2}$, indicating the presence of additional bodies in the system. We find that a resonant solution clearly improves the quality of purely Keplerian fit (Figure 4). Assuming a stellar mass of 1.1 $M_\odot$, the best-fit masses of the putative resonant planets are $m_b = 3.2 \pm 0.4 m_J$ and $m_c = 1.1 \pm 0.3 m_J$ with $P_b = 509 \pm 15$ days and $P_c = 254.5$ days (P_c is not a free parameter in our resonant model). Since only 19 data points are available, we agree with F07 that more data are required to disentangle the true nature of this system.

To quantify how significant is the resonant solution with respect to the eccentric one, we compute the empirical FAP as described in the previous section. For this experiment, we use the square root of the reduced χ^2, (i.e., $\sqrt{\bar{\chi}^2}$) to enable direct comparison with F07. $\sqrt{\bar{\chi}^2}$ differs from $\sqrt{\chi^2}$ used in Section 3.1 by a constant multiplicative factor which is not relevant for the FAP estimations because the number of free parameters in the our resonant model is equal to the number of parameters of a single-planet Keplerian solution. In this case, we use the published uncertainties and the a nominal stellar jitter of 2.0 m s^{-1} to weight each observation and compute the $\sqrt{\bar{\chi}^2}$. Since the FAP is very small, we produce one million Monte Carlo realizations of the data. The histogram of the obtained $\sqrt{\bar{\chi}^2}$ is shown in Figure 5. In 350 out of one million cases, the resonant solution gives a better $\sqrt{\bar{\chi}^2}$ than our best fit 1.64, obtaining a FAP of 0.035%.

Table 5
Statistical Results from Our Sample of Exoplanets

Solution Type	Number of Cases	Fraction
Total	176	100%
Circular	71	40%
Non-circular	105	60%
Eccentric	38	22%
Resonant	4	∼2%
Undecided	63	36%

We perform the same experiment but assuming an exact resonant orbit, adding noise, and fitting a Keplerian orbit for another set of one million MC realizations. In this case, the Monte Carlo generated distribution of the $\sqrt{\bar{\chi}^2}$ peaks at 3.5 very close to the $\sqrt{\bar{\chi}^2}$ published in F07. This indicates that the obtained $\sqrt{\bar{\chi}^2} = 3.6$ by F07 is compatible with the confusion of a resonant system with an eccentric planet. We have repeated the experiment introducing different levels noise (from the nominal 2.0 m s^{-1} to 10 m s^{-1}), obtaining very small FAP in all cases.

Therefore, we find strong statistical evidence to support the hypothesis that HD 125612 has a pair of planets in the 2:1 resonance instead of a single eccentric planet. It clearly exemplifies how the degeneracy under discussion and how the natural bias to the eccentric orbital solutions can be affecting a good number of exoplanet discoveries.

Finally, the dynamical stability of the system has been checked by numerical orbital integrations up to 1 Myr using Mercury (Chambers 1999). The integration of HD 125612 shows that the candidate resonant planets would be in a strongly interacting regime where one of the resonant critical arguments circulates and the other one has a large libration amplitude. However, the system remained stable and no close encounters occurred. Since the orbital solution is poorly constrained, more data are required to further constrain the orbital parameters and ensure the long-term stability of the system. The resulting Doppler signal as a function of time is illustrated in Figure 6. In the figure, it can be seen that the dynamical interactions between planets will have obvious effects on the Doppler signal in timescales as short as a few orbital periods (∼10 yr).

A small linear trend is required to obtain a good fit of the data (in both Keplerian and resonant cases), which is too large to be explained by the newly discovered M4V companion. This indicates the presence of an additional very long period and massive planet in the system. We strongly encourage the follow-up of this system.

4. DYNAMICAL STABILITY

As illustrated in the discussion of HD 125612b, a question that needs to be addressed is whether the 2:1 resonant configurations in Table 1 are, in general, dynamically stable. Several 2:1 resonant multi-planet systems have already been found (i.e., GJ 876, HD 82943, HD 73526, HD 128311). Dynamical stability of 2:1 resonant configurations has also been discussed by several authors. For example, Lee & Peale (2002) show that resonant locking may arise naturally during the migration of exoplanets in the presence of a protoplanetary disk. The case where the outer planet is significantly more massive has been recently

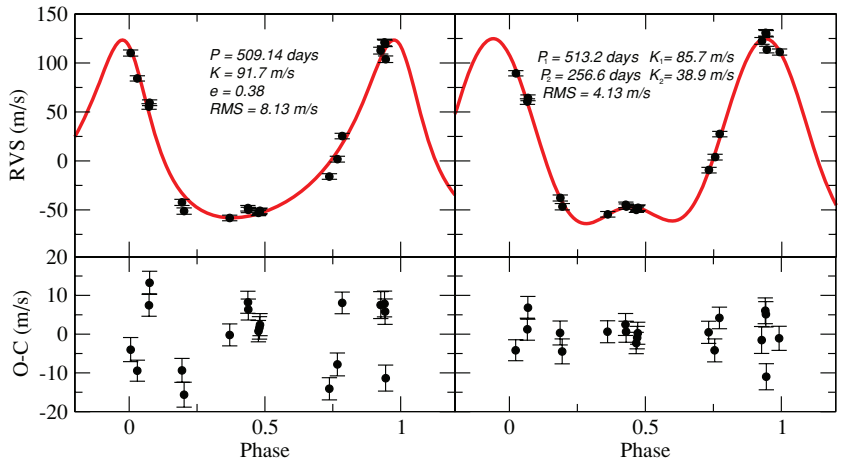

Figure 4. Phased representation of the eccentric (left) and resonant (right) solutions for system HD 125612. Assuming a stellar jitter of 2.0 m s^{-1}), the square root of the reduced χ^2 is $\sqrt{\bar{\chi}^2}_{\rm ecc} = 3.58$ for the eccentric solution and $\sqrt{\bar{\chi}^2}_{\rm res} = 1.64$ for the resonant one. The residuals of each fit (bottom) clearly illustrate the reduction of the dispersion in the resonant solution case.

(A color version of this figure is available in the online journal.)

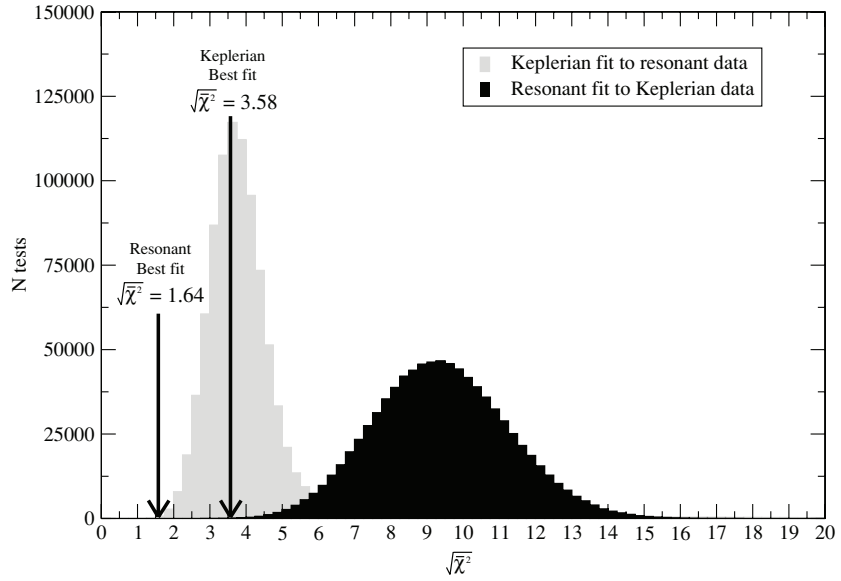

Figure 5. Histograms of the Monte Carlo generated distributions of $\sqrt{\bar{\chi}^2}$. Black bars are the result of fitting a resonant model to the MC realizations of the Keplerian solution. Our obtained solution has a $\sqrt{\bar{\chi}^2} = 1.64$ clearly smaller than the typical $\sqrt{\bar{\chi}^2}$ obtained adding noise to the Keplerian model. Gray bars correspond to Keplerian fits to resonant simulated data. This time the distribution peaks at 3.5 very close to the best Keplerian fit to the real data.

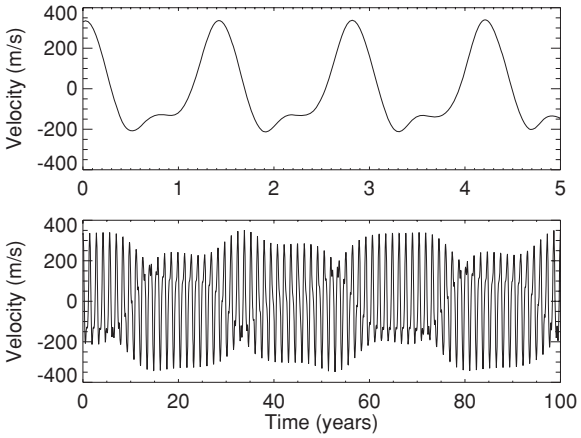

Figure 6. Radial velocity signal as obtained by numerical integration of the three-body problem in HD 125612. Significant differences in the shape of the signal start to be evident in timescales of ∼10 yr.

discussed in great detail by Michtchenko et al. (2008), concluding that long-term stability is guaranteed and that the resonant capture during migration is particularly favored. Therefore, there is no theoretical objection to the case addressed in this paper; in contrast, recent work strongly supports the existence and stability of $k_2 \ll k_1$ systems in 2:1 resonant configurations.

Eccentric hot Neptunes ($m_1 \sin i < 50\ m_\oplus$) are particularly interesting since their potentially hidden companions are of a few Earth masses or less (see Table 2). Their small Ke^2 makes it difficult to distinguish between solutions with the current instrumental accuracies, but these are excellent targets to seek out for the effects of dynamical interactions. A very tantalizing case is the four-planet system around GJ 581 (Mayor et al. 2009b) where the inner body is of a few Earth masses and the new published solution for the exterior planet (GJ 581d) gives an eccentricity of 0.4. A resonant planet hidden in the eccentric solution of GJ 581d would perfectly fill the current gap between the 12 day orbit of GJ 581c and 66 day orbit

of GJ 581d. The potential candidate would be of a few Earth masses (∼2–3 $M_\oplus$) and would lie in the middle of the habitable zone. Recent dynamical studies (Zollinger & Armstrong 2009) considering all the planets except the small inner one strongly support the stability of the system when adding a few Earth-mass planet in a fairly broad range of orbital configurations around the 2:1 resonance with GJ 581d. Since the inner planet is very small and in a very tight orbit, the authors do not expect these results will change too much. Given the RMS for GJ 581(∼1.46 m s^{-1}), an amplitude of the second harmonic for GJ 581d of 0.4 m s^{-1} and ignoring the dynamical interactions, the number of observations required to reach an $S/N_{(2)}$ of 4.32 and disentangle the degeneracy is ∼280. Compared to the current 110 observations, this number could be achieved in near future.

5. BREAKING THE DEGENERACY

The question now becomes: how to observationally identify eccentric imposters. We focus here on the Doppler and photometric methods, which are the only two techniques with currently enough sensitivity to discern between both cases. In the future, techniques such as astrometry and direct imaging will be useful as well.

5.1. Using Improved Doppler Data

As discussed in previous sections, the most direct approach is to increase the number of radial velocity observations, $N_{\rm obs}$, and their precision $\sigma_{\rm obs}$, until the condition $S/N_{(2)} > 4.32$ is satisfied. It is important to recall that the actual limit in pushing the accuracy $\sigma_{\rm obs}$ is currently put by stellar jitter that can be of the order of 2–5 m s^{-1} even for relatively quiet stars. We suspect that some of the undecided solutions in Figure 3 over the critical line of 4.32 are most likely dominated by stellar jitter or poorly sampled making still undecidable which solution is favored.

The phase of maximal difference will depend on each particular combination of orbital parameters and has to be examined case by case by direct inspection of the best Keplerian solution compared to the best resonant one by subtracting both fitted models. As a general rule, the differences will be more obvious near the quadratures of the resonant solution, that is, around the extremes of the Doppler curve and at the quadratures of the inner candidate seen as little bumps on the resonant signal (dashed line) in Figure 2.

This strategy works better when the initial one-planet fit suggests a relatively large eccentricity $e > 0.3$ and a poor initial fit. An example of this situation was the discovery of the planetary system around GJ 876. This system was initially confused with a single planet (Delfosse et al. 1998; Marcy et al. 1998) in an $e \sim 0.31$ orbit. Additional observations revealed a system of two resonant planets with smaller eccentricities and in a strong interaction regime (Marcy et al. 2001). Further observations and detailed numerical integration of the *N*-body problem by Laughlin & Chambers (2001) confirmed the presence of the two massive eccentric bodies and uncovered an additional very short period companion (Rivera et al. 2005).

Therefore, in the case of planets in a strongly interacting regime (see Section 3.2), the numerical integration of the orbits provides a powerful discrimination method and can be used to predict the timescale required to observe the dynamical effects which should be observed in the case of a resonant configuration.

5.2. Photometric Methods

A second approach is to use photometric observations. These can confirm or discard the presence of a second planet in some circumstances, either by detection of planetary transits and occultations, or by observing reflected light or thermal emission from the planets. Photometric methods are mostly efficient for planets in short-period orbits, since those tend to be hot and have a higher probability of transiting in front of their star. Assuming that the period P, the eccentricity e, and τ_0 are known from the Doppler solution and that the orbital inclination of the planet is close to 90° (edge on), the predicted instant of transit $T_{\rm I}$ depends on the eccentricity as

$$T_{\rm I} = \tau_0 + NP\,\frac{1}{4} - \frac{e\,P\cos\omega}{\pi} + O(e^2), \qquad (6)$$

where N is the number of integer periods elapsed from τ_0. If the system contains a hidden companion, then the true e will be small and the transit will occur almost exactly $1/4\ P$ after crossing the line of nodes. This test is only significant if τ_0 is well constrained. An unambiguous determination of the eccentricity is obtained when both the primary transit and the occultation (planet passes behind the star) can be observed. This is because the time interval between these two events is independent of τ_0. If the orbit is circular, the occultation occurs half-period after the transit. If the orbit of the planet is truly eccentric, the time difference between the transit $T_{\rm I}$ and the occultation $T_{\rm II}$ is

$$T_{\rm II} - T_{\rm I} = \frac{P}{2} + 2\,\frac{e\,P\cos\omega}{\pi} + O(e^2), \qquad (7)$$

which can be as large as several hours on some of the known transiting planets.

A representative example where the observation of transits brakes the degeneracy is GJ 436. The star hosts a hot Neptune in an eccentric orbit ($e \sim 0.14$) with a period of only 2.63 days (Maness et al. 2007). The potential hidden companion would have a mass as low as 2.5 $m_\oplus$. GJ 436b was recently found to transit (Gillon et al. 2007), but because of the uncertainty in τ_0, the detection of the primary transit alone was not sufficient to confirm the eccentric orbit. Shortly after, the occultation was observed in thermal emission with the *Spitzer* telescope at the instant predicted by an eccentric solution (Deming et al. 2007). If the orbit of GJ 436b had been circular, the time of the occultation would differ by 3 hr from the observed time and would not be detected with the *Spitzer* observations.

6. CONCLUSIONS

We show that the Doppler signal of a single eccentric planet can mimic the signal of a two-planet system in a 2:1 circular or near-circular resonant orbit. This degeneracy is affecting a large fraction of the known exoplanets, this is, around 30%–40% of the published single-planet systems. We also find strong evidence of at least one case (HD 125612) where the resonant solutions are significantly better than the published eccentric one by Fischer et al. (2007). The analysis described in this paper can also be applied to multi-planet systems with eccentric candidates, where the degree of degeneracy is expected to be similar or even stronger due to the mixed signals of the different planets involved. The detailed analysis of multi-planetary systems is more complex and usually involves dynamical stability consideration. Therefore, a case-by-case study is imposed. A remarkable example is the planetary system

around GJ 581 (Mayor et al. 2009b) where a 2–3 Earth mass planet could be hidden in the habitable zone of the system.

The only techniques currently able to distinguish between two resonant planets and single eccentric planet systems are limited to the Doppler and photometric approaches described above. In the future, other methods, such as astrometry and direct imaging, will also provide ways to uncover eccentric imposters (see Moorhead & Ford 2009). Astrometry will be the first one to become sensitive enough, once the upcoming space astrometric missions *Gaia*/ESA (Lindegren et al. 2008, to be launched in 2011) and SIM/NASA (Unwin et al. 2008, to be launched after 2015), go online. High precision astrometry will be most helpful if the resonant orbits are not coplanar. Otherwise, it will suffer from the same degeneracies as the Doppler technique (Konacki et al. 2002). The ultimate test will be direct imaging, which will make possible to measure whether the orbit of the detected planet is indeed eccentric. This will have to wait until space-borne missions such as a Darwin/*Terrestrial Planet Finder* launch.

The conclusions of this work make it worth reconsidering some published orbital solutions and motivate the follow-up of some interesting systems. We find that future announcements of eccentric planets should be carefully tested before publication, since it is relatively simple to check if there is any improvement using a resonant configuration. Also, we find that several reported radial velocity curves (Mayor et al. 2009a, 2009b) may contain hidden signals of rocky planets.

G.A.E. thanks A. Boss and A. Weinberger for financial support. M.L.M. acknowledges support provided by NASA through Hubble Fellowship grant HF-01210.01-A awarded by the STScI, which is operated by the AURA, Inc., for NASA, under contract NAS5-26555. J.E.C. thanks NASA's Origins of Solar Systems Program for support. We also thank A. Bonanos and all the other members of the Astronomy group at CIW-DTM for fruitful discussions. The authors also recognize the comments and suggestions made by L. Lucy and an anonymous referee which helped to improve the manuscript significantly.

REFERENCES

Bean, J. L., McArthur, B. E., Benedict, G. F., Harrison, T. E., Bizyaev, D., Nelan, E., & Smith, V. V. 2007, AJ, 134, 749
Boss, A. P. 1997, Science, 276, 1836
Butler, R. P., Marcy, G. W., Williams, E., Hauser, H., & Shirts, P. 1997a, ApJ, 474, L115
Butler, R. P., Marcy, G. W., Williams, E., Hauser, H., & Shirts, P. 1997b, ApJ, 474, L115
Chambers, J. E. 1999, MNRAS, 304, 793
Cumming, A. 2004, MNRAS, 354, 1165
Cumming, A., Butler, R. P., Marcy, G. W., Vogt, S. S., Wright, J. T., & Fischer, D. A. 2008, PASP, 120, 531
Delfosse, X., et al. 1998, A&A, 338, L67
Deming, D., et al. 2007, ApJ, 667, L199
Fischer, D. A., et al. 2007, ApJ, 669, 1336
Fischer, D. A., et al. 2008, ApJ, 675, 790
Ford, E. B. 2006, ApJ, 642, 505
Ford, E. B., Lystad, V., & Rasio, F. A. 2005, Nature, 434, 873
Gillon, M., et al. 2007, A&A, 472, L13
Giuppone, C. A., et al. 2009, ApJ, 699, 1321
Ida, S., & Lin, D. N. C. 2004, ApJ, 604, 388
Konacki, M., & Maciejewski, A. J. 1996, Icarus, 122, 347
Konacki, M., & Maciejewski, A. J. 1999, ApJ, 518, 442
Konacki, M., Maciejewski, A. J., & Wolszczan, A. 2002, ApJ, 567, 566
Laughlin, G., & Chambers, J. E. 2001, ApJ, 551, L109
Lee, M. H., & Peale, S. J. 2002, ApJ, 567, 596
Lindegren, L., et al. 2008, in IAU Symp. 248, A Giant Step: from Milli- to Micro-arcsecond Astrometry, ed. W. Jin, I. Platais, & M. A. C. Perryman (Cambridge: Cambridge Univ. Press), 217
Lucy, L. B. 2005, A&A, 439, 663
Lucy, L. B., & Sweeney, M. A. 1971, AJ, 76, 544
Maness, H. L., et al. 2007, PASP, 119, 90
Marcy, G. W., & Butler, R. P. 1996, ApJ, 464, L147
Marcy, G. W., Butler, R. P., Vogt, S. S., Fischer, D., & Lissauer, J. J. 1998, ApJ, 505, L147
Marcy, G. W., et al. 2001, ApJ, 556, 296
Marcy, G. W., et al. 2002, ApJ, 581, 1375
Mayor, M., & Queloz, D. 1995, Nature, 378, 355
Mayor, M., et al. 2009a, A&A, 493, 639
Mayor, M., et al. 2009b, A&A, 507, 487
McArthur, B. E., et al. 2004, ApJ, 614, L81
Meschiari, S., et al. 2009, PASP, 121, 1016
Michtchenko, T. A., Beaugé, C., & Ferraz-Mello, S. 2008, MNRAS, 387, 747
Moorhead, A., & Ford, E. B. 2009, AAS/Division of Dynamical Astronomy Meeting, Vol. 40, BAAS, 41, 889
Moulton, F. R. 1914, An Introduction to Celestial Mechanics (2nd ed; New York: MacMillan)
Mugrauer, M., & Neuhäuser, R. 2009, A&A, 494, 373
Pepe, F., et al. 2007, A&A, 462, 769
Pollack, J. B., et al. 1996, Icarus, 124, 62
Press, W. H., Teukolsky, S. A., Vetterling, W. T., & Flannery, B. P. 1992, Numerical Recipes in FORTRAN. The Art of Scientific Computing (2nd ed.; Cambridge: Cambridge Univ. Press)
Rivera, E. J., et al. 2005, ApJ, 634, 625
Soderhjelm, S. 1975, A&A, 42, 229
Thommes, E. W., Bryden, G., Wu, Y., & Rasio, F. A. 2008, ApJ, 675, 1538
Unwin, S. C., et al. 2008, PASP, 120, 38
Ward, W. R. 1997, Icarus, 126, 261
Zollinger, R., & Armstrong, J. C. 2009, A&A, 497, 583